ISSN: 2621-4709 E-ISSN: 2621-2528
Journal of Applied Agricultural Science and Technology
Vol. 10 No. 3 (2026): 414-438

Assessing the Effectiveness of Object-Based Image Analysis in Mapping High Visual Similarity Objects from Conventional Drone Imagery (A Case Study: The Maturity Level of Sago)

Iriansa [a,*], Mutmainnah [b], Masluki [b], Andi Jumardi [a], Ichwan Muis [a], Budi Utomo Putra Azis [c], Erwin Amri [d]

[a] Informatics Study Program, Faculty of Computer Engineering, Universitas Cokroaminoto Palopo, Palopo, Indonesia
[b] Agrotechnology Study Program, Faculty of Agriculture, Universitas Cokroaminoto Palopo, Palopo, Indonesia
[c] Environmental Engineering Study Program, Faculty of Engineering, Universitas Teknologi Sulawesi, Makassar, Indonesia
[d] Urban and Regional Planning Study Program, Faculty of Engineering, Universitas Bosowa, Makassar, Indonesia

Abstract. *Conventional unmanned aerial vehicle (UAV) Red–Green–Blue (RGB) imagery offers a cost-effective alternative for precision agriculture; however, its limited spectral separability constrains classification when target classes exhibit high visual similarity, particularly in non-cultivated areas with dense vegetation. Maturity assessment of sago palm (Metroxylon sagu Rottb.) exemplifies this challenge: identification of the harvestable stage remains dependent on labour-intensive field inspection, and delayed identification causes stem mortality and yield loss. This study evaluated an Object-Based Image Analysis (OBIA) framework for discriminating three sago maturity levels (Young, Harvestable and Overripe) based on an RGB orthomosaic and a Digital Surface Model (DSM) over a 9-hectare non-cultivated site in Wailawi, North Luwu, Indonesia, using a DJI Phantom 4 Pro quadcopter at an altitude of 50 m. Multiresolution segmentation generated 6,210 crown-level objects, classified by Random Forest under two configurations: a five-feature set and a seventeen-feature set optimised through Recursive Feature Elimination (RFE). Evaluation used 600 independent objects (200 per class) from the testing partition through stratified random sampling, re-labelled by visual interpretation, with 95% confidence intervals from 1,000 bootstrap resamples. The seventeen-feature model outperformed the baseline, yielding Overall Accuracy of 93.00% (95% CI: 91.00–94.83) versus 89.00% (86.83–91.50), Macro-F1 of 92.92% versus 88.92% and Cohen's Kappa of 0.895 (0.860–0.922) versus 0.835 (0.795–0.873). Classification uncertainty concentrated on the Young–Harvestable boundary, whereas the Overripe class was consistently discriminated (F1 = 98.77%). Visible-band spectral statistics, GLCM and GLDV texture descriptors and DSM-derived structural features contributed most to accuracy, while geometric descriptors showed marginal influence. The framework established a robust and economically accessible pathway for operational sago maturity monitoring.*

Keywords: *agriculture technology; machine learning classification; remote sensing; RGB imagery; sago palm maturity.*

Type of the Paper: Regular Article.

https://doi.org/10.55043/jaast.v10i3.536
Received December 6, 2025; Received in revised form May 14, 2026; Accepted May 16, 2026; Published **Articles in Press**
* Corresponding author
Email: iriansa@uncp.ac.id

1. Introduction

Sago palm (*Metroxylon sagu* Rottb.) constitutes a strategic carbohydrate-yielding commodity with substantial contributions to food security in Indonesia, particularly across the regions of Papua, Maluku, Sulawesi and Sumatra [1–3]. The plant exhibits high productivity potential, with dry starch yields per stem reaching up to 1 tonne [4], and demonstrates considerable ecological adaptability to marginal lands [5]. Despite these potentials, the persistently low adoption of precision-based management practices within sago production systems [6] continues to suppress productivity and weaken the position of sago within the national agricultural value chain [7,8]. A principal operational bottleneck lies in the identification of crop maturity, which, to date, remains dependent on manual field observation through morphological indicators such as stem height, stem diameter, leaf number and the presence of inflorescences [9,10]. This conventional approach is labour-intensive, susceptible to observer subjectivity and difficult to scale across extensive landscapes [11], particularly in non-cultivated sago stands where canopy density is high, plant distribution is irregular and physical accessibility is constrained [12,13]. Consequently, the optimal harvest phase is frequently overlooked, resulting in numerous stems undergoing senescence prior to harvest, which ultimately increases yield losses and threatens long-term production sustainability [14–16].

Recent advances in unmanned aerial vehicle (UAV/drone) technology have substantially expanded the operational scope of precision agriculture, particularly through the integration of multispectral and hyperspectral sensors for fine-scale crop condition monitoring [17–19]. UAV-based remote sensing has demonstrated considerable utility across a wide range of agricultural applications, including the detection of physiological stress [20], biomass estimation [21], plant disease mapping [22] and the assessment of fruit maturity [23]. Nevertheless, the high acquisition cost of multispectral and hyperspectral sensors continues to constitute a principal barrier to widespread deployment among smallholder farmers and in resource-limited regions [24]. This condition reinforces the position of UAVs equipped with conventional Red–Green–Blue (RGB) cameras as the most economically accessible alternative for routine vegetation monitoring. However, RGB imagery is inherently limited in spectral separability, a constraint that frequently compromises the reliability of pixel-based classification approaches when applied to spectrally complex vegetation [25]. To address this methodological limitation, Object-Based Image Analysis (OBIA) has emerged as a robust analytical framework, owing to its capacity to exploit not only spectral attributes but also textural, geometric and contextual descriptors at the object level [26–28]. The integration of multi-dimensional object-based features enables OBIA to partially compensate for the spectral limitations of RGB imagery, thereby enhancing classification reliability in operational vegetation mapping [29–32].

The effectiveness of integrating UAV RGB imagery with OBIA has been extensively documented across a broad range of vegetation mapping applications. Reported overall classification accuracies approach 96% in land cover classification [33], wetland vegetation mapping [34] and dead-wood detection within forest environments [35]. In crop-specific contexts, RGB–OBIA workflows have similarly produced high performance, achieving 99% accuracy in olive tree detection and enumeration [36] and 95% in the discrimination of pistachio developmental stages [37]. Such high-performance outcomes are generally obtained under conditions in which target objects exhibit strong visual contrast against the surrounding background, spatial distribution patterns are relatively regular and spectral interference from co-occurring vegetation remains minimal. The classification of sago maturity levels in non-cultivated stands departs substantially from these ideal conditions. Adjacent maturity classes display pronounced visual similarity in canopy colour, leaflet morphology and crown texture; canopy density tends to be high, and stem distribution is markedly irregular [38]. These conditions intensify intra-class variability and promote spectral mixing with surrounding vegetation, ultimately reducing inter-class separability when RGB imagery is employed in isolation, and thereby limiting the direct transferability of the accuracy levels previously reported in less complex landscapes.

Although the scientific literature on UAV-based vegetation classification continues to expand rapidly, no prior investigation has systematically evaluated the use of OBIA for mapping sago maturity levels using conventional UAV RGB imagery in non-cultivated dense canopies. Existing sago-related remote sensing studies have predominantly focused on species-level detection or stand-area inventory, rather than phenological discrimination among maturity levels exhibiting high visual similarity. The present study sought to address this gap by hypothesising that an OBIA framework integrating spectral, textural, geometric and Digital Surface Model (DSM)-derived structural features is capable of discriminating three sago maturity levels (Young, Harvestable and Overripe) at the object level with an overall classification accuracy exceeding 90%, based solely on a UAV RGB orthomosaic. To systematically test this hypothesis, three research questions were formulated: (i) which combination of multiresolution segmentation parameters generates the most stable crown-level objects in dense and irregular sago stands; (ii) which categories of object-based features contribute most substantially to the discrimination of maturity levels, and to what extent does feature reduction preserve overall classification accuracy; and (iii) how do classification performance and class-wise error structure differ across classification models employing various feature combinations. Addressing these questions provides empirical evidence concerning the operational feasibility of low-cost UAV-based monitoring of sago maturity levels, while simultaneously offering transferable methodological

guidance for other vegetation mapping problems characterised by high visual similarity.

2. Materials and Methods

2.1. Time and Location of the Research

This study was conducted in 2025 within non-cultivated sago stands located in Wailawi Village, West Malangke District, North Luwu Regency, South Sulawesi Province, Indonesia. Field observation and drone RGB imagery acquisition covered approximately 9 ha (Fig. 1).

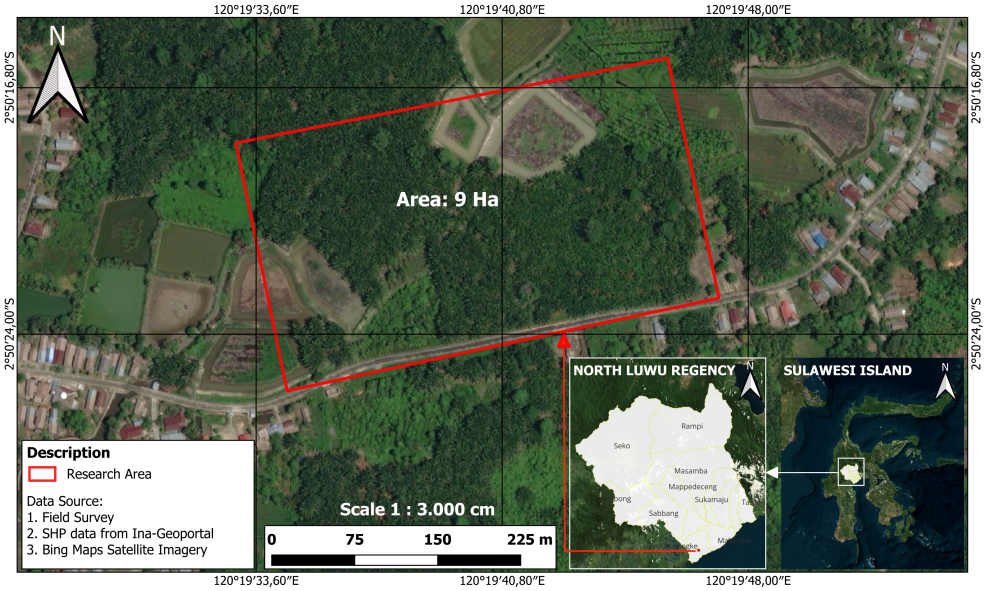

Fig. 1. Research Location in Wailawi Village, North Luwu Regency, South Sulawesi Province.

2.2. Field Observation and Data Acquisition

Field observation was conducted to establish object-level reference labels for sago maturity. A total of 29 sample plots were selected purposively to represent the range of maturity conditions present at the study site. Plot coordinates were recorded using a Garmin GPSMAP 64s receiver, and sago maturity was assessed through morphological indicators associated with the local growth phases. Following Osozawa et al. [39], who systematically documented the local growth phases of sago palm within the same sub-district, the observed phases were consolidated into three sago maturity levels (SMLs): "Young", "Harvestable" and "Overripe" (Fig. 2). The field-derived SML labels were subsequently linked to segmented image objects to construct the object-level reference dataset used for supervised classification and accuracy assessment.

Aerial data acquisition was performed using a DJI Phantom 4 Pro quadcopter equipped with a 1-inch CMOS RGB sensor (20-megapixel effective resolution, 5,472 × 3,648 pixels), a 24-mm focal length equivalent in 35 mm format, a variable aperture ranging from f/2.8 to f/11 and a mechanical shutter operating between 8 s and 1/2,000 s. Image acquisition was conducted under clear-sky conditions around midday (approximately 11:00 to 12:30 local time, WITA) to minimise elongated shadow effects and bidirectional reflectance variability. A double-grid flight pattern, executed across four orthogonal directions, was applied to reduce shadow-induced spectral

variability and to enhance the geometric robustness of photogrammetric reconstruction. Flight missions were planned and executed using the PIX4Dcapture Pro application, with the UAV operated at 50 m above ground level, 90% forward overlap, 70% lateral overlap and a camera tilt angle of 70°. This acquisition configuration produced an RGB orthomosaic with an approximate spatial resolution of 1 cm. Very high spatial resolution imagery is methodologically advantageous for OBIA workflows, as it enhances both object delineation and the extraction of object-level features in spectrally complex vegetation scenes [41].

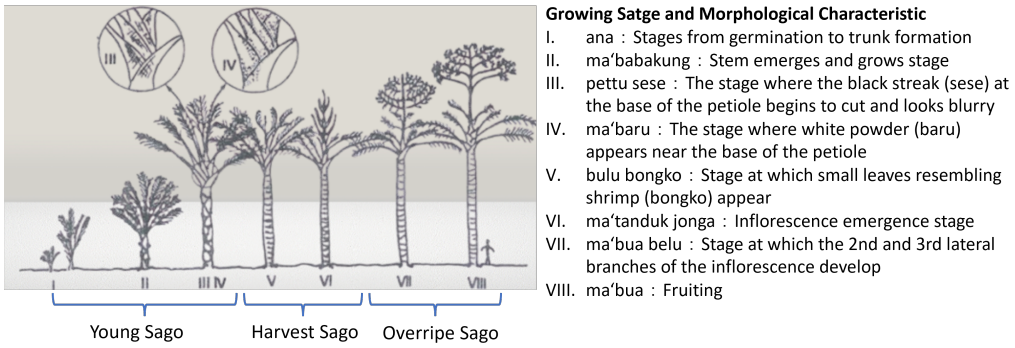

Fig. 2. Classification of SMLs based on the phases of sago plant growth [40].

2.3. Orthomosaic and DSM Generation

Photogrammetric processing was conducted using Agisoft Metashape Professional v2.1.1. From an initial set of 1,316 acquired photographs, 10 images were excluded due to misalignment, resulting in 1,306 photographs retained for processing. Image alignment was executed in a high-quality setting, with key point and tie point limits maintained at their default values of 40,000 and 4,000, respectively. Sparse point cloud quality was subsequently inspected to identify and correct alignment inconsistencies, including misalignment and geometric distortion. A dense point cloud was generated in a high-quality setting with mild-depth filtering applied to preserve canopy edge information while suppressing isolated outliers. Mesh and texture reconstruction were then performed to produce a detailed representation of the canopy surface structure.

The RGB orthomosaic was generated using the Build Orthomosaic function, producing geometrically consistent imagery at an approximate spatial resolution of 1 cm. The Digital Surface Model (DSM) was generated from the dense point cloud using the Build DEM function at an approximate spatial resolution of 4 cm, providing elevation information encompassing both canopy and other surface elements [42]. A 3 × 3 median filter was applied to the DSM to attenuate residual noise without over-smoothing crown-level micro-topographic variation. The integration of very high-spatial resolution orthomosaic imagery with DSM-derived height information has been reported to enhance the discrimination of vegetation objects, particularly under conditions in which the spectral separability of RGB imagery is constrained [43].

2.4. Object-Based Image Segmentation

Image segmentation constitutes a core component of OBIA and substantially influences classification performance [44]. Segmentation was performed in eCognition Developer v10.4, which supports raster-based object generation and object-level feature extraction [45]. A top-down segmentation approach was implemented using the Multiresolution Segmentation (MRS) algorithm [46], a region-growing procedure governed by three principal parameters (scale, shape and compactness) that jointly determine object size, boundary adherence and within-object spectral and geometric homogeneity [47].

To minimise subjectivity in determining the scale parameter, the Estimation of Scale Parameter 2 (ESP2) tool was applied. ESP2 identifies candidate optimal scales based on peaks in the rate of change (ROC) of local variance (LV) [48], thereby supporting a systematic, data-driven parameter selection process in contrast to purely trial-and-error approaches [49]. The segmentation procedure was executed simultaneously across four image layers (Red, Green, Blue and DSM), with equal layer weights (1.0) retained to preserve both spectral and structural information during crown delineation. The final MRS parameter values, together with the rationale underlying their selection, are summarised in Table 1.

The reported parameter values were calibrated specifically for non-cultivated sago stands at an approximately 1-cm ground sampling distance (GSD) and a 50-m flight altitude. Direct transfer of these values to other landscapes, sago varieties or different acquisition resolutions is not advisable, as optimal MRS parameters are strongly dependent on canopy size, scene complexity and image resolution. ESP2-guided recalibration of the scale parameter, together with sensitivity testing of shape and compactness, is therefore recommended when the workflow is applied to new sites.

Table 1. Final MRS parameters used for object-based image segmentation.

Parameter	Value	Selection rationale
Scale	1701	Selected from ESP2 candidate peaks; produced integrated, crown-level objects
Shape	0.2	Tested from 0.1 to 0.9; balanced fragmentation control without crown over-merging
Compactness	0.5	Default; sensitivity testing showed negligible effects on object count and morphology
Layer Weights	R = G = B = DSM = 1.0	Equal weighting to retain spectral and structural cues for crown delineation

2.5. Feature Extraction and Selection

Multi-feature integration has been shown to improve OBIA-based classification performance by enabling segmented objects to be characterised through multiple complementary descriptors [41]. However, the use of large feature sets without appropriate feature selection

procedures may introduce redundancy and increase computational cost [50], whereas only a limited subset of features typically contributes substantially to model performance [31,32].

An initial set of 22 object-level features was therefore defined (Table 2). Feature extraction yielded 6,210 image objects across the 9-hectare study area, all of which were labelled into the three SML categories through visual interpretation using the 29 field reference plots as morphological references. The labelled object pool was subsequently partitioned through stratified random sampling into a training set (70%) and a testing set (30%).

Feature evaluation and ranking were performed using a Random Forest (RF) classifier combined with Recursive Feature Elimination (RFE). All 22 features were evaluated sequentially by incrementally adding one feature at a time and observing the corresponding changes in classification accuracy, resulting in 22 feature combination schemes. RFE subsequently established the relative importance ranking of each feature according to its contribution to classification accuracy [51,52]. Based on this ranking, two feature configurations were defined and compared: (i) a minimal configuration consisting of the highest-ranked features and (ii) an optimal configuration corresponding to the feature subset in which classification accuracy reached its peak.

Table 2. Description of the feature variables to be used in SML classification.

Feature Type	Variable	Information	Source
Vegetation Index (VI)	Red Intensity	The value of redness intensity, normalized as $R/(R+G+B)$	[53]
	Green Intensity	The value of greenness intensity, normalised as $G/(R+G+B)$	
	Blue Intensity	The value of blueness intensity, normalised as $B/(R+G+B)$	
	EXG	The excess green index, calculated as $2G-R-B$	
	TGI	An index that estimates the area of the triangle bounding the leaf reflectance spectrum, the corner points being the center wavelengths of the RGB sensor, calculated as $G-(0.39\times R)-(0.61\times B)$	[54]
	VDVI	The vegetation index of light difference used to replace NDVI variables, calculated as $(2G-B-R)/(2G+B+R)$	[55]
Spectral Values (RGB)	Mean (R, G, B), StandDev (R, G, B) and MaxDifference	R (red), G (green) and B (blue) are the component color channels of the imagery, where each pixel is represented by a digital number.	[31]
Geometry	Asymmetry, Shape Index and Compactness	The geometric characteristics of an object, calculated based on the spatial arrangement of the constituent pixels	
Texture	GLCM Dissimilarity, GLCM Mean, GLCM Correlation and GLDV Contrast	The intensity of brightness variation between adjacent pixels in the image, calculated based on the Gray Level Co-occurrence Matrix (GLCM) and Gray Level Difference Vector (GLDV)	[32]
Information of Height	Mean DSM and StandDev DSM	The mean and standard deviation for each object, calculated based on DSM data	

2.6. Supervised Classification

SML classification was performed using the Random Forest (RF) algorithm, a machine-learning classifier widely employed for vegetation mapping and reported to perform robustly relative to several alternative classifiers in comparable contexts [31, 32,56–58]. RF constructs an ensemble of decision trees and aggregates their predictions, thereby enabling the model to capture non-linear relationships and interactions among object-level features extracted from the RGB orthomosaic and DSM layers [59].

Classification was implemented through the built-in RF module of eCognition Developer v10.4, configured with the following hyperparameters: number of trees (ntree) set to 100, maximum tree depth left unrestricted, number of features evaluated at each split (mtry) set to the square root of the total number of input features, Gini impurity as the split criterion and minimum node size set to 1. These settings correspond to the standard configuration commonly adopted in object-based vegetation classification studies, balancing predictive performance with computational efficiency.

Model training was performed using labelled objects derived from the 70% training partition described in Section 2.5, with each training object assigned to one of the three SML classes according to the field reference labels. The minimal and optimal feature configurations identified through RFE (see Section 2.5) were trained and evaluated in parallel, after which the resulting models were applied to all segmented objects across the study area to produce object-based SML classification maps.

2.7. Accuracy Test

Classification accuracy was assessed at the object (segment) level using 600 independent reference objects (200 per class), drawn from the 30% testing partition through stratified random sampling and re-labelled by visual interpretation to ensure independence from the training data. Accuracy was evaluated through a confusion matrix comparing predicted SML classes against the independent reference labels, from which Overall Accuracy (OA) and Producer Accuracy (PA) were derived [52]. Complementary metrics computed from the same matrix included User Accuracy (UA, equivalent to precision), Class-wise F1-score, Macro-averaged F1-score (Macro-F1) and Balanced Accuracy. Cohen's Kappa and a multi-class form of Matthew’s Correlation Coefficient (MCC) were additionally employed as robust agreement measures under potential class imbalance.

Statistical uncertainty was quantified using a stratified bootstrap resampling procedure with 1,000 iterations, in which validation objects were resampled with replacement within each class to preserve the original class proportions. The 2.5^{th} and 97.5^{th} percentiles of the resulting bootstrap distributions defined the lower and upper bounds of the 95% confidence intervals (CIs). The

minimal and optimal feature configurations were compared within this same validation framework to ensure methodological consistency.

3. Results and Discussion

3.1. Results

3.1.1. Field Observation Results

Field observation yielded 29 independent sample plots, comprising 10 Young, 14 Harvestable and 5 Overripe sago stands (Fig. 3). The plots were spatially referenced to the UAV RGB orthomosaic to characterise the visual cues associated with each SML class and to support both segmentation quality evaluation and the labelling of training and testing objects.

Visual characterisation revealed distinct morphological patterns across the three classes. Young sago typically exhibits greener foliage, with leaflets arranged tightly along the rachis and leaf sheaths appearing slimmer and more upright; consequently, crown boundaries are often difficult to delineate within dense stands. Harvestable sago is characterised by marginal leaf yellowing, sparser leaflet appearance and fronds extending more horizontally, with trees generally taller and crowns wider than those of the Young class. Overripe sago is the most readily identifiable class owing to the emergence of inflorescences with whitish-grey coloration and visibly reduced leaf density [38]. These morphological cues served as the primary reference for evaluating segmentation results and for guiding the labelling of training and testing samples.

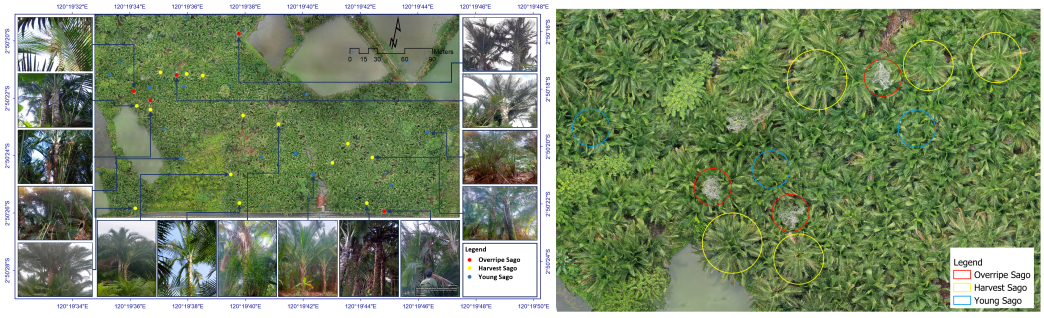

(a) (b)

Fig. 3. (a) Independent sample plot; (b) visual appearance of stand trees for each SML class from UAV RGB imagery.

3.1.2. Image Segmentation Results

Multiresolution Segmentation (MRS) was applied across four input layers (Red, Green, Blue and DSM). Given that the SML classes share partial similarity in crown colour and form, segmentation evaluation focused on crown-area heterogeneity and object coherence to ensure that individual crowns were delineated as integrated objects. ESP2 analysis identified three candidate segmentation scales (Fig. 4). Levels 1 (scale = 363) and 2 (scale = 911) produced highly fragmented crown objects, indicating over-segmentation and an increased risk of partitioning within-class crowns into multiple objects, which may propagate inconsistency into subsequent

classification [60]. In contrast, Level 3 (scale = 1701) generated more integrated and compact crown objects that better preserved within-class crown integrity, and was therefore adopted for further parameter testing.

Sensitivity testing was subsequently conducted for the shape and compactness parameters at scale = 1701. Shape was varied from 0.1 to 0.9, while compactness was held constant at 0.5. As summarised in Fig. 5, increasing the shape value systematically reduced the number of segmented objects, reflecting the progressive merging of small fragments into larger and smoother objects, consistent with the MRS trade-off in which higher shape weighting attenuates spectral-driven fragmentation and enhances geometric regularisation [61]. Visual inspection (Fig. 6a) further confirmed that a very low shape value (0.1) retained fragmented objects in Harvestable stands, while higher values improved object coherence. However, excessively high shape values induced under-segmentation in Young sago areas through merging of adjacent crowns under dense canopy conditions. A shape value of 0.2 was, therefore, selected as the balanced setting that minimised fragmentation without introducing extensive crown merging.

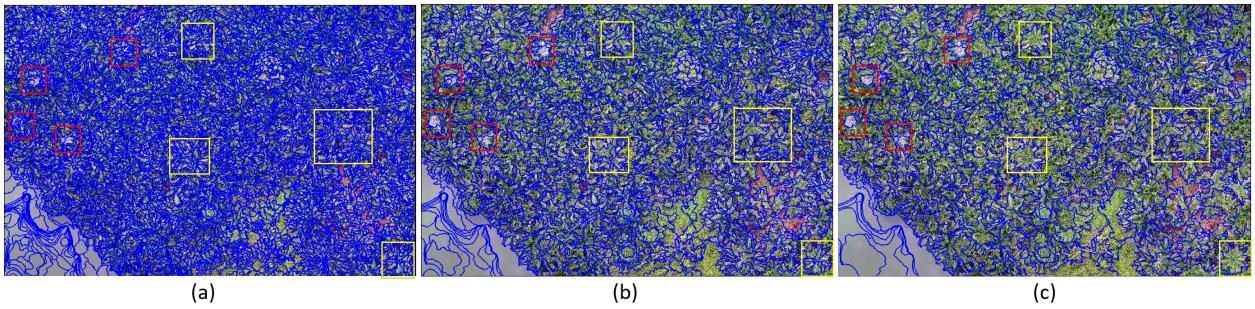

Fig. 4. Results of image segmentation by using ESP2 tools; (a). Level 1 with Scale 363; (b) Level 2 with Scale 911; (c) Level 3 with Scale 1701; Harvestable sago (yellow square); and Overripe sago (red square).

Compactness was then varied while holding scale = 1701 and shape = 0.2. As shown in Fig. 5 and visually supported by Fig. 6b, variation in compactness produced no meaningful differences in either the number of segmented objects or the overall boundary configuration of crown objects. Compactness, therefore, contributed minimally to segmentation variability for the present SML mapping task and was retained at the default value of 0.5 for full-area MRS implementation.

Although quantitative segmentation metrics such as Intersection over Union (IoU), the Dice coefficient or the Segmentation Quality Index were not directly computed in the present study, segmentation reliability was indirectly substantiated through three complementary mechanisms: (i) data-driven scale parameter selection through ESP2, which minimised subjectivity in manual parameter tuning; (ii) systematic sensitivity analysis across the shape and compactness parameter ranges, which confirmed the stability of the adopted configuration and (iii) downstream classification accuracy, which served as a holistic indicator of segmentation reliability under operational conditions [62]. The explicit integration of pixel-overlap-based segmentation quality

metrics, supported by manually delineated reference crowns, is recommended for future research to enable a more rigorous geometric assessment of object delineation.

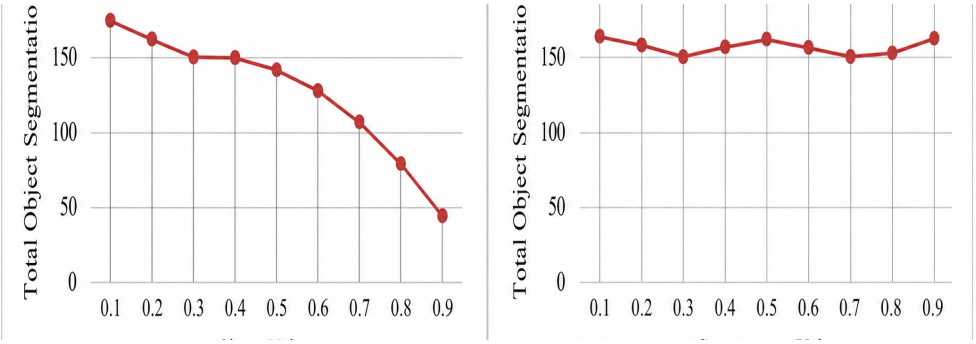

Fig. 5. Effects of shape and compactness settings on the number of segmented objects (scale = 1701).

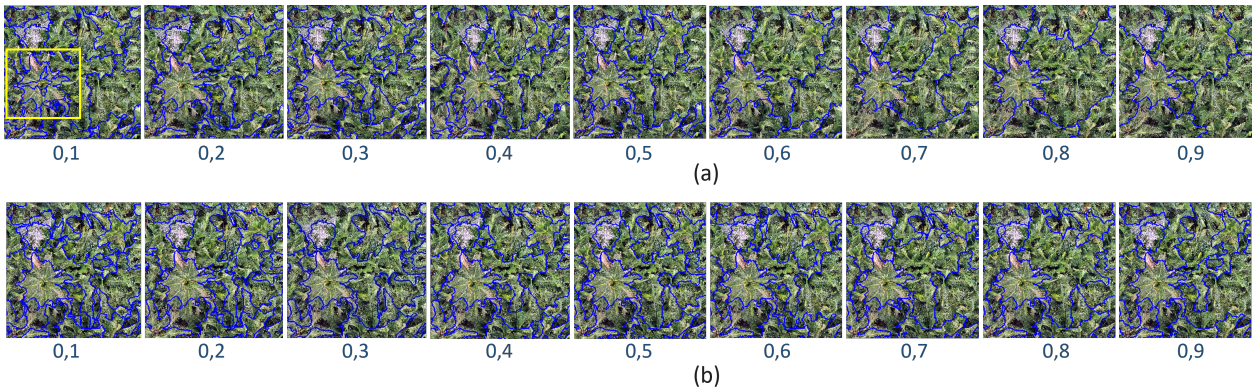

Fig. 6. Effects of object segmentation on a.) the variation of shape parameter values (scale 1701, compactness 0.5) and b.) the variation of compactness parameter values (scale 1701, shape 0.2).

3.1.3. Feature Evaluation and Selection Results

Feature evaluation was performed by sequentially adding features during RF training on the training subset, yielding 22 classification schemes (Fig. 7). Overall Accuracy (OA) increased with the number of features, with a marked improvement within the first five features (Scheme 5: 89.11%). Subsequent additions produced smaller gains with local peaks at Scheme 10 (91.12%) and Scheme 14 (91.53%). The highest OA was obtained at Scheme 17 (91.93%), beyond which additional features yielded no meaningful improvement, indicating performance stabilisation.

Based on this evaluation, RFE established the relative importance ranking of all 22 features (Fig. 8). The five highest-ranked variables were Mean Green, GLDV Contrast, Mean Red, GLCM Mean and Mean DSM, indicating that spectral, texture, and DSM-derived height information collectively supported SML discrimination under complex canopy conditions. The five lowest-ranked variables (Green Intensity, Asymmetry, StandDev DSM, Compactness and Shape Index) contributed marginally and were excluded from the optimal subset. The ranking accordingly defined two configurations for full-area classification: a minimal configuration comprising the five highest-ranked features and an optimal configuration comprising the seventeen-feature subset associated with peak OA.

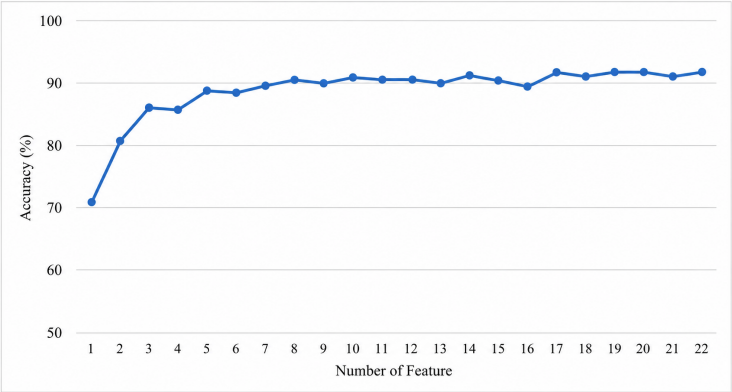

Fig. 7. Effects of feature addition to the accuracy of classification results of the RF model on the training subset area.

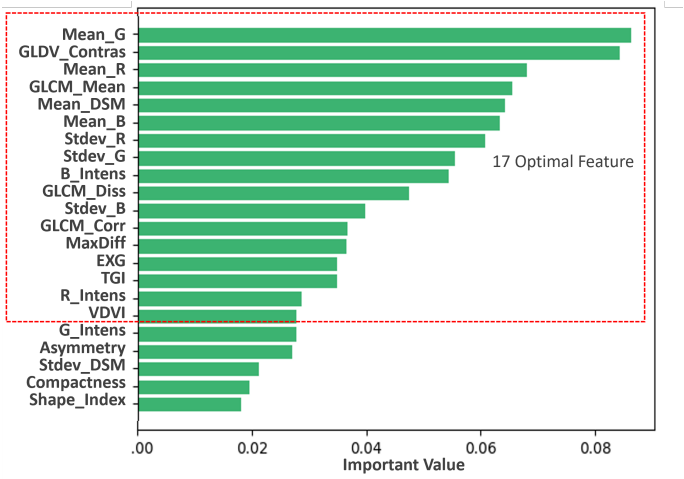

Fig. 8. Results of feature variable ranking using the RFE model.

3.1.4. Results of SML Classification

Full-area classification performance was evaluated under the minimal (five-feature) and optimal (seventeen-feature) configurations using 600 independent reference objects (200 per class). In the confusion matrices (Table 3 and Table 4), rows correspond to field-derived reference classes and columns to predictions from the RF classifier; User Accuracy (UA) is reported as precision.

The optimal configuration consistently outperformed the minimal configuration across all object-based metrics, with OA increasing from 89.00% to 93.00%, Macro-F1 from 88.92% to 92.92% and Cohen's Kappa from 0.835 to 0.895 (Table 5). Class-wise gains were most pronounced for the Young (F1: 84.80% to 91.00%) and Harvestable (F1: 83.20% to 89.01%) classes, whereas the Overripe class remained stable at the upper bound of performance (F1 = 98.77%, PA = 100.00%). The dominant residual error consistently occurred between the Young and Harvestable classes, reflecting their pronounced visual similarity in RGB imagery under dense-canopy conditions.

Bootstrap-derived 95% confidence intervals (CIs), computed from 1,000 stratified resamples, confirmed that the observed gains were statistically meaningful. The optimal-

configuration CIs for OA (91.00–94.83%) and Macro-F1 (90.86–94.81%) did not overlap with the corresponding point estimates of the minimal configuration (89.00% and 88.92%, respectively), supporting the conclusion that the improvement was not attributable to sampling variability (Table 4).

Table 3. Confusion matrix of SML classification results with the five most important variables.

Reference \ Predicted	Young	Harvestable	Overripe	PA
Young	173	26	1	86.50%
Harvestable	35	161	4	80.50%
Overripe	0	0	200	100.00%
UA	83.17%	86.10%	97.56%	
OA				89.00%

Table 4. Confusion matrix of SML classification results with 17 optimal variables.

Reference \ Predicted	Young	Harvestable	Overripe	PA
Young	192	7	1	96.00%
Harvestable	30	166	4	83.00%
Overripe	0	0	200	100.00%
UA	86.49%	95.95%	97.56%	
OA				93.00%

Table 5. Summary of object-based performance metrics with 95% bootstrap confidence intervals (1,000 stratified resamples) for the minimal and optimal feature configurations.

Metric	5 Features	17 Features
Overall Accuracy (OA)	89.00%	93.00%
Macro-F1	88.92%	92.92%
Balanced Accuracy	89.00%	93.00%
F1 – Young	84.80%	91.00%
F1 – Harvestable	83.20%	89.01%
F1 – Overripe	98.77%	98.77%
Cohen's Kappa	0.835	0.895
Matthew's Correlation Coefficient (MCC)	0.835	0.897

3.1.5. Comparison of Classified Areas and Spatial Distribution

Beyond accuracy metrics, the stability of mapped class extents is operationally important, as management decisions often depend on area estimates for each maturity class. Switching from the minimal to the optimal configuration affected only the Young and Harvestable classes (Table 6); the Young area decreased by 914 m², while the Harvestable area increased by an equivalent magnitude, indicating that part of the area previously assigned to the Young class was reclassified as Harvestable under the richer feature representation. The Overripe class remained stable at 159 m² across both configurations, in line with the consistent discriminability of Overripe sago.

Table 6. Total comparison of classification areas for every SML class under two classification schemes.

SML Class	Classification Area		Difference (m^2)
	5 Variables (m^2)	17 Variables (m^2)	
Young Sago	44,877	43,962	-914
Harvest Sago	7,320	8,235	+914
Overripe Sago	159	159	0
Total	52,356	52,356	

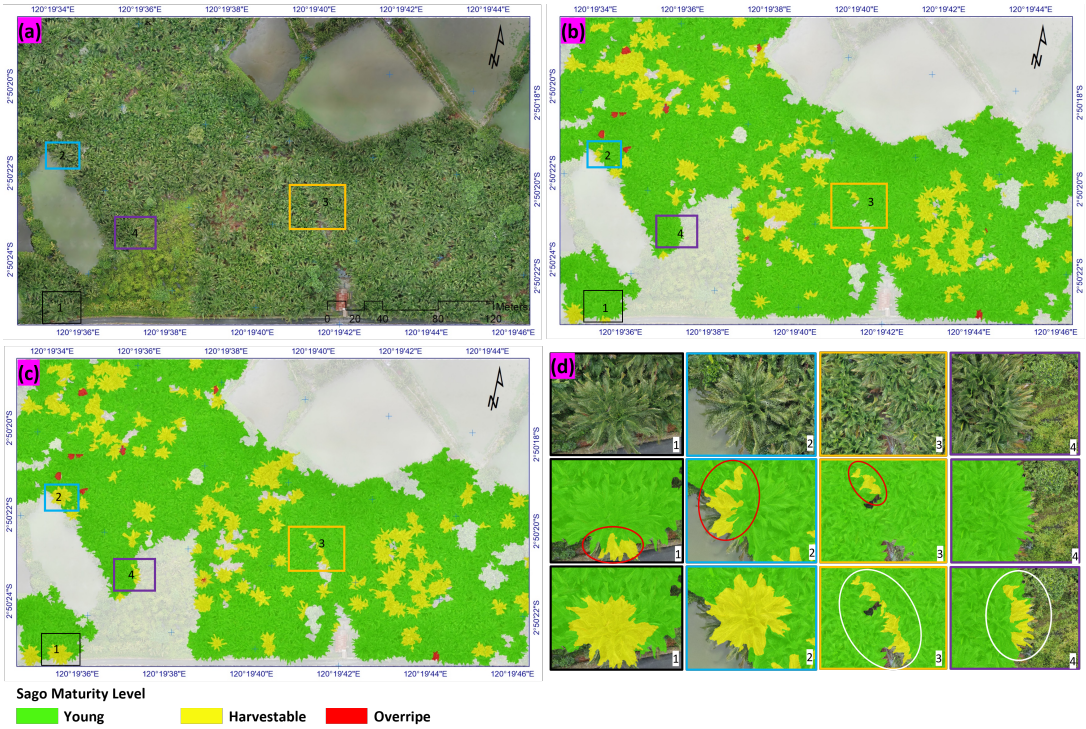

Fig. 9. Classification maps: (a) UAV RGB orthomosaic of the study area; (b) SML classification using the minimal (five-feature) configuration; (c) SML classification using the optimal (seventeen-feature) configuration; (d) cropped focus area indicated by the rectangle in (a–c), in which red circles mark misclassification locations under the minimal configuration, and white circles mark misclassification locations under the optimal configuration.

At the map scale, the two classification outputs exhibit broadly consistent spatial patterns (Fig. 9b–c), with Young and Harvestable stands constituting the dominant classes across the study area and Overripe stands appearing as sparse, localised objects. A closer inspection of representative stands (Fig. 9d) indicated that the optimal configuration delineated Harvestable crowns more completely, reducing the partial crown labelling observed under the minimal configuration. In Fig. 9d, misclassification locations under the minimal configuration are marked with red circles, while those under the optimal configuration are marked with white circles, enabling a direct visual comparison of error locations between the two models. This pattern is consistent with the higher precision and F1-score obtained for the Harvestable class (Table 4), suggesting that texture- and DSM-derived descriptors provide additional discriminatory power beyond visible-band colour alone. Localised class switching between the Young and Harvestable classes, however, persisted in stands exhibiting a transitional canopy appearance (e.g., fronds with partial yellowing), reflecting a realistic ambiguity in RGB-based maturity discrimination under dense-canopy conditions.

The overlay change map in Fig. 10 explicitly identifies the spatial reallocation between the two configurations. The disagreement pattern is dominated by reciprocal transitions between the Young and Harvestable classes, consistent with the dominant misclassification observed in the confusion matrices (Table 3 and Table 4), and aligns with the 914-m² net shift recorded in Table

6. Overall, the richer feature representation primarily refined class allocation on the Young–Harvestable boundary, without altering the broader spatial distribution of maturity classes across the study area.

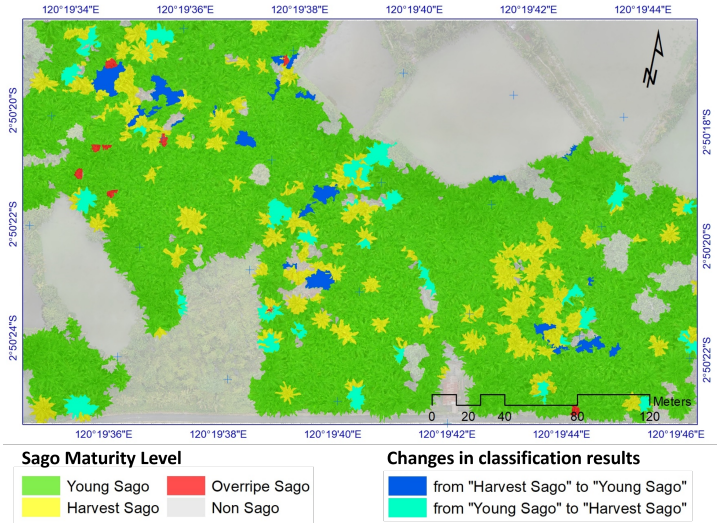

Fig. 10. Spatial reallocation between the minimal (five-feature) and optimal (seventeen-feature) classification outputs, illustrating the dominant Young-to-Harvestable transitions.

3.2. Discussion

This study demonstrates that Object-Based Image Analysis, OBIA, can enhance the operational utility of conventional drone RGB orthomosaics for precision agriculture, particularly when the target classes are difficult to separate using pixel-based spectral information alone. Although RGB imagery lacks the NIR and SWIR bands that are generally more sensitive to vegetation biochemical and physiological variations [63], OBIA mitigates this limitation by operating on segmented objects and integrating complementary descriptors such as spectral statistics, texture, geometry and height-related features [64]. This capability is especially relevant for sago maturity mapping in non-cultivated stands, where dense canopy conditions and irregular spatial patterns increase within class variability and promote spectral mixing effects.

3.2.1. Segmentation behaviour and parameter justification

The results confirm that MRS parameterisation, particularly scale and shape, strongly controls object granularity and boundary delineation, which in turn affect downstream classification performance (Fig. 4, Fig. 5 and Fig. 6). ESP2-driven scale selection produces relatively high candidate scales, an outcome consistent with the very high spatial resolution of the orthomosaic and the multilayer segmentation design that includes both RGB and DSM, which collectively increase local variance and may lead to excessive fragmentation under smaller-scale settings [31,65]. The principle that scale selection should be guided by the intended mapping unit, scene complexity and objective scale estimation tools has been reaffirmed in recent OBIA studies of agricultural and natural vegetation [66,67]. Higher shape values progressively reduced fragmentation and improved object compactness, but excessively high values induced under-

segmentation in dense Young stands. The selected value of 0.2 minimised fragmentation without merging adjacent crowns, which aligns with the recommendation in [61] that shape should be tuned to balance the spectral–geometric trade-off inherent in MRS. Compactness variation produced negligible differences in object morphology, consistent with the observation that compactness exerted a weaker influence on segmentation outcomes than scale and shape when the input layers were sufficiently informative [68]. Overall, the selected configuration is defensible because it prioritises crown-level object integrity in a challenging non-cultivated setting and aligns with the well-established principle that segmentation quality is a primary determinant of OBIA classification reliability in complex vegetation scenes [62,69].

3.2.2. Feature dominance and biophysical interpretation

The RFE-based ranking and the comparison between the minimal and optimal configurations provide direct insight into which feature categories most strongly support SML discrimination. The five highest-ranked variables consisted of two visible-band statistics (Mean Green and Mean Red), two texture descriptors (GLDV Contrast and GLCM Mean) and one structural descriptor (Mean DSM), indicating that effective discrimination requires the joint contribution of spectral, textural and height information rather than reliance on a single feature family. The spectral dominance of Mean Green and Mean Red can be interpreted biophysically. As sago palms progress through phenological stages, foliage colour shifts from vivid green in Young stands towards yellowish-green tones in Harvestable stands, consistent with the changes in canopy reflectance during palm maturation reported in recent UAV RGB analyses of related palm species [70]. The contribution of GLDV Contrast and GLCM Mean reflects the role of within-crown brightness heterogeneity, which differs systematically among maturity classes because of differences in leaflet density, frond inclination and shadow distribution within the crown; the central role of texture in discriminating spectrally similar vegetation has been repeatedly demonstrated [32,64]. The high importance of Mean DSM confirms that structural cues (notably the differential canopy heights of Harvestable versus Young stems documented in field observations) provide independent discriminatory information that RGB alone cannot supply. By contrast, the marginal contribution of geometric descriptors (Asymmetry, Compactness and Shape Index) is unsurprising given that crown morphology in non-cultivated sago is highly irregular and that segmentation outcomes vary across canopy density gradients, conditions under which geometric statistics tend to lose discriminatory power [52].

3.2.3. Performance gains and comparison with alternative approaches

The transition from the minimal to the optimal configuration produced consistent gains across all object-based metrics (OA from 89.00% to 93.00%, Macro-F1 from 88.92% to 92.92% and Cohen's Kappa from 0.835 to 0.895), and the non-overlapping bootstrap CIs (Table 5) indicate

that the improvement is statistically meaningful rather than an artefact of sampling variability. The Overripe class remained reliably classified across both configurations (F1 = 98.77%, PA = 100.00%) because the emergence of whitish-grey inflorescences produced strong spectral and textural contrasts that were readily captured even by the parsimonious feature set. The dominant residual confusion on the Young–Harvestable boundary reflects the fundamental spectral and textural overlaps between adjacent maturity stages and represents a realistic limitation of RGB-only mapping under dense-canopy conditions. The 93% OA reported here is consistent with the upper tier of recent OBIA–RF benchmarks using UAV imagery for vegetation mapping: 96% for wetland vegetation classification with multi-feature OBIA [32], 95% for pistachio developmental stage discrimination [37] and OA in the 87–97% range for OBIA–RF land cover and vegetation succession mapping with multispectral UAV inputs [71]. The reported accuracy also exceeds the typical 80–88% range achieved by pixel-based RGB classifiers in spectrally complex vegetation [25,72]. Relative to deep-learning approaches such as CNN-based crown delineation, which has reached high accuracy in forest canopy mapping [73,74], the present OBIA–RF workflow trades a modest accuracy ceiling for interpretability, lower computational cost and feature-level transparency, all of which are operationally important for deployment in resource-constrained settings.

3.2.4. Operational implications for sago production systems

From an operational perspective, the OBIA–RF framework offers a viable pathway for low-cost, scalable monitoring of sago maturity in non-cultivated stands. The principal practical advantages are threefold. First, conventional RGB UAVs are substantially more affordable and easier to deploy than multispectral or hyperspectral platforms [24], which makes the workflow accessible to smallholder farmers, extension officers and local agricultural agencies. Second, the workflow is reproducible because each processing stage relies on widely available tools and well-documented parameters (Agisoft Metashape for photogrammetric reconstruction, eCognition Developer for segmentation and classification and ESP2 for objective scale parameter selection). Third, the object-based outputs are directly relevant to harvest planning: the spatial distribution of Harvestable crowns can guide field crews to target harvest-ready stems before they progress to the Overripe stage, thereby reducing pre-harvest stem senescence and associated yield losses. Recent UAV-based studies in tree–crop systems have similarly demonstrated that RGB–OBIA outputs can directly support precision management decisions in low-input production contexts [36,75,76].

3.2.5. Limitations and future research directions

Despite these strengths, the present study has limitations that warrant explicit acknowledgement and frame the agenda for further work. First, validation was restricted to a single study site and a single acquisition date in October 2025; consequently, extrapolation of the reported

accuracy levels to other locations or to other acquisition periods should be made with caution. Second, the acquisition was conducted in the dry-to-wet season transition, and seasonal variations of canopy moisture, leaf turgor and background reflectance may have altered both segmentation behaviour and class separability; multi-temporal validation across the full wet–dry seasonal cycle is, therefore, required to establish year-round operational robustness, in line with recommendations from recent meta-analyses on UAV vegetation classification [77]. Third, all flights were conducted around solar noon (11:00–12:30 WITA) under clear-sky conditions to minimise shadow effects; the sensitivity of classification accuracy to lower solar elevation angles, oblique illumination and partial cloud cover therefore remains untested, although the influence of illumination geometry on UAV vegetation classification has been well documented [78,79]. Fourth, the dataset represented the local Kapa landrace of *Metroxylon sagu* Rottb. and the prevailing canopy structure of North Luwu; varieties such as Roe, Pulu, Para, Tuni or Molat, which differ in canopy density, leaflet arrangement and crown morphology [80], are likely to require recalibration of MRS parameters and possibly retraining of the RF classifier. Fifth, the geometric quality of segmentation was not quantified through pixel-overlap-based metrics (e.g., IoU, the Dice coefficient or the Segmentation Quality Index) due to the absence of manually delineated reference crowns; future research should incorporate such metrics, supported by independent crown digitisation, to enable a more rigorous geometric evaluation of object delineation. Building on these limitations, future research priorities should include: (i) multi-site, multi-temporal and multi-variety validation; (ii) controlled assessment of illumination-geometry sensitivity; (iii) integration of multispectral or canopy-height-model inputs as a benchmark against the present RGB-only framework and (iv) systematic benchmarking of OBIA–RF against deep-learning crown delineation pipelines, under matched validation protocols, to identify the operational regimes in which each approach is most cost-effective.

4. Conclusions

This study establishes three principal findings regarding the use of Object-Based Image Analysis (OBIA) for sago maturity mapping in non-cultivated dense canopies. First, the integrated OBIA framework can overcome the well-known limitation of RGB-only imagery in discriminating visually similar vegetation classes, achieving an Overall Accuracy of 93% in a setting characterised by high inter-class visual similarity. Second, effective discrimination requires the joint contribution of spectral, textural and DSM-derived structural information rather than reliance on any single feature family, as evidenced by the dominance of these three modalities among the highest-ranked feature variables. Third, contrary to the conventional emphasis on geometric descriptors in object-based classification, such variables contribute marginally under non-

cultivated conditions, reflecting the irregular crown morphology and density-dependent segmentation variability inherent in natural sago stands.

The proposed framework enables rapid identification of harvestable sago with 93% accuracy using off-the-shelf RGB drones, potentially reducing harvest losses through timely maturity mapping. By eliminating the need for specialised multispectral sensors or high-performance computing infrastructure, the workflow is directly accessible to smallholder farmers, extension officers and agricultural agencies in eastern Indonesia, where its primary operational value lies in supporting harvest scheduling and minimising pre-harvest stem senescence. Future research should prioritise multi-site, multi-temporal and multi-variety validation, alongside systematic benchmarking against multispectral and deep-learning approaches, to consolidate the operational generalisability of the framework across varied agro-ecological contexts.

Abbreviations

OBIA	Object-Based Image Analysis
OA	Overall Accuracy
RGB	Red Green Blue
DSM	Digital Surface Model
DOM	Digital Orthomosaic Model
DEM	Digital Elevation Model
SML	Sago Maturity Level
ROC	Rate of Change
LV	Local Variance
MRS	Multi-Resolution Segmentation
ESP2	Estimation of Scale Parameter 2
RF	Random Forest
RFE	Recursive Feature Elimination
PA	Producer Accuracy
UA	User Accuracy
MCC	Matthews Correlation Coefficient
PSE	Potential Segmentation Error
NSR	Number-of-segments Ratio
ED2	Euclidean Distance 2
CI	Confidence Interval
GSD	Ground Sampling Distance
GLCM	Gray Level Co-occurrence Matrix
GLDV	Gray Level Difference Vector

Data Availability Statement

All relevant data supporting the findings of this study have been fully presented within the article. However, should reviewers or other interested parties require additional data for verification or further clarification, such information can be made available upon request. Data requests may be directed to the corresponding author via email at: iriansa@uncp.ac.id.

CRediT Authorship Contribution Statement

Iriansa: Conceptualization, methodology, formal analysis, writing original draft

preparation, supervision, project administration, and funding acquisition. **Mutmainnah**: Formal analysis, investigation, writing review and editing, visualization. **Masluki**: Validation, investigation. **Andi Jumardi**: Software, data curation. **Budi Utomo Putra Azis**: methods and acquisition of drone imagery.

Declaration of Competing Interest

The authors of this manuscript declare no conflict of interest or competing interest

Declaration of Use of AI in the Writing Process

The author(s) used ChatGPT Plus during the preparation of this manuscript to [e.g., improve grammar, paraphrase text]. After using the tool/service, the author(s) carefully reviewed and edited the content and take full responsibility for the content of the publication.

Acknowledgement

The publication of this article was funded by the Ministry of Higher Education, Science, and Technology of the Republic of Indonesia.

References

[1] Dewayani W, Suryani, Arum RH, Septianti E. Potential of sago products supporting local food security in South Sulawesi. IOP Conf Ser Earth Environ Sci 2022;974:012114. https://doi.org/10.1088/1755-1315/974/1/012114.

[2] Sidiq FF, Coles D, Hubbard C, Clark B, Frewer LJ. Sago and the indigenous peoples of Papua, Indonesia: A review. Journal of Agriculture and Applied Biology 2021;2:138–49. https://doi.org/10.11594/JAAB.02.02.08..

[3] Yusuf DN, Sutariati GAK. The potential of sago as a local food ingredient to support the food security in South Konawe. IOP Conf Ser Earth Environ Sci 2021;807:022077. 10.1088/1755-1315/807/2/022077

[4] Djoefrie MHB, Pembayun P, Baka LR. Sago Production Potential in Several Regions in Indonesia. The 14th International Sago Symposium SAGO 2023 TOKYO, 2024;23. https://www.sagopalmsociety.com/_files/ugd/3f58e5_398fcb790b40418ab832df78c76a3039.pdf#page=28

[5] Puspantari W, Cahyana PT, Saepudin A, Budiyanto B, Kurniasari I, Kusumasmarawati AD, et al. Sago Rice as an Environmentally Sustainable Food. BIO Web Conf EDP Sciences 2023;69:03012. https://doi.org/10.1051/bioconf/20236903012

[6] Fetriyuna F, Letsoin SMA, Jati IRAP, Purwestri RC. Potential of Underutilized Sago for Bioenergy Uses. Int J Adv Sci Eng Inf Technol 2024;14:144–50. https://doi.org/10.18517/IJASEIT.14.1.19202.

[7] Tampubolon AP, Turjaman M, Osaki M. Sago Palm Practice as Natural AeroHydro Culture. Tropical Peatland Eco-Management 2021:363–77. https://doi.org/10.1007/978-981-33-4654-3_12/COVER.

[8] Yumeina D, Kasmira K, Makkarennu M. Effect of heat moisture treatment on psychochemical modification of sago starch. AIP Conf Proc AIP Publishing 2023;2596. https://doi.org/10.1063/5.0119495

[9] Lim LWK, Chung HH, Hussain H, Bujang K. Sago Palm (Metroxylon sagu Rottb.): Now and Beyond. Pertanika J Trop Agric Sci 2019;42:435–51. https://www.researchgate.net/publication/333650292_Sago_Palm_Metroxylon_sagu_Rottb_Now_and_Beyond

[10] Syafiuddin M, Zubair H, Jayadi M, Baharuddin B, Busthanul N. The potential for developing sago-taro intercropping in South Sulawesi: a review. IOP Conf Ser Earth Environ Sci 2021;681:012039. https://doi.org/10.1088/1755-1315/681/1/012039.

[11] Wahed Z, Joseph A, Zen H, Kipli K. Sago Palm Detection and its Maturity Identification Based on Improved Convolution Neural Network. Pertanika J Sci Technol 2022;30:1219–36. https://doi.org/10.47836/PJST.30.2.20.

[12] Markus Rawung JB, Indrasti R. The Constraints to Sago Development and Improvement Efforts in Siau Tagulandang Biaro (Sitaro) Islands. E3S Web of Conferences 2021;232:01029. https://doi.org/10.1051/E3SCONF/202123201029.

[13] Nurlette AR, Mukson, Sumekar W. Sustainable Management of Sago (Metroxylon Spp) Agroindustry in East Indonesia. The International Journal of Social Sciences World (TIJOSSW) 2021;3:33–45. https://doi.org/10.5281/zenodo.5131391.

[14] Ellen R. How Nuaulu sago palms feature in debates around the measurement of plant use and valuation. The Cultural Value of Trees Routledge 2022:177–90. https://doi.org/10.4324/9780429320897

[15] Pue AG, Fletcher MT, Blaney B, Greenhill AR, Warner JM, Latifa A, et al. Addressing food insecurity in Papua New Guinea through food safety and sago cropping. Sago Palm: Multiple Contributions to Food Security and Sustainable Livelihoods 2018:123–37. https://doi.org/10.1007/978-981-10-5269-9_9

[16] Konuma H. Status and outlook of global food security and the role of underutilized food resources: Sago palm. Sago Palm: Multiple Contributions to Food Security and Sustainable Livelihoods 2018:3–16. https://doi.org/10.1007/978-981-10-5269-9_1/FIGURES/7

[17] Sabir RM, Mehmood K, Sarwar A, Safdar M, Muhammad NE, Gul N, et al. Remote sensing and precision agriculture: a sustainable future. Transforming agricultural management for a sustainable future: climate change and machine learning perspectives, Springer 2024;75–103. https://doi.org/10.1007/978-3-031-63430-7_4

[18] Guebsi R, Mami S, Chokmani K. Drones in precision agriculture: A comprehensive review of applications, technologies, and challenges. Drones 2024;8:686. https://doi.org/10.3390/drones8110686

[19] Kar D, Dhal SB. Advancing food security through drone-based hyperspectral imaging: applications in precision agriculture and post-harvest management. Environ Monit Assess 2025;197:283. https://doi.org/10.1007/s10661-025-13650-1

[20] Yang Q, Shi L, Han J, Yu J, Huang K. A near real-time deep learning approach for detecting rice phenology based on UAV images. Agric For Meteorol 2020;287:107938. https://doi.org/10.1 016/j.agrformet.2020.107938

[21] Tatsumi K, Igarashi N, Mengxue X. Prediction of plant-level tomato biomass and yield using machine learning with unmanned aerial vehicle imagery. Plant Methods 2021;17:1–17. https://doi.org/10.1186/s13007-021-00761-2

[22] Plata IT, Panganiban EB, Alado DB, Taracatac AC, Bartolome BB, Labuanan FRE. Drone-based geographical information system (GIS) mapping of cassava pythoplasma disease (CPD) for precision agriculture. Int J Emerg Technol Adv Eng 2022;12:1–9. https://www.researchgate.net/publication/358377530_Drone-based_Geographical_Information_System_GIS_Mapping_of_Cassava_Pythoplasma_Disease_CPD_for_Precision_Agriculture

[23] Ojo IA, Costa L, Ampatzidis Y, Alferez F, Shukla S. Citrus fruit maturity prediction utilizing UAV multispectral imaging and machine learning. 2021 ASABE Annual International Virtual Meeting, American Society of Agricultural and Biological Engineers; 2021;1. https://doi.org/10.13031/aim.202100495

[24] Cheng M-F, Mukundan A, Karmakar R, Valappil MAE, Jouhar J, Wang H-C. Modern Trends and Recent Applications of Hyperspectral Imaging: A Review. Technologies (Basel) 2025;13:170. https://doi.org/10.3390/technologies13050170

[25] Sohl MA, Mahmood SA, Rasheed MU. Comparative performance of four machine learning models for land cover classification in a low-cost UAV ultra-high-resolution RGB-only orthomosaic. Earth Sci Inform 2024;17:2869–85. https://doi.org/10.1007/s12145-024-01318-2

[26] Šupčík A, Oršulová V. Using OBIA for detection of canopy and row-gap by using drone images in vineyards. Precision agriculture'21, Wageningen Academic Publishers; 2021, p. 531–7. https://doi.org/10.3920/978-90-8686-916-9_82

[27] Ventura D, Napoleone F, Cannucci S, Alleaume S, Valentini E, Casoli E, et al. Integrating low-altitude drone based-imagery and OBIA for mapping and manage semi natural grassland habitats. J Environ Manage 2022;321:115723. https://doi.org/10.1016/j.jenvman.2022.115723

[28] Ye Z, Yang K, Lin Y, Guo S, Sun Y, Chen X, et al. A comparison between Pixel-based deep learning and Object-based image analysis (OBIA) for individual detection of cabbage plants based on UAV Visible-light images. Comput Electron Agric 2023;209:107822. https://doi.org/10.1016/j.compag.2023.107822

[29] Deur M, Gašparović M, Balenović I. An evaluation of pixel-and object-based tree species classification in mixed deciduous forests using pansharpened very high spatial resolution satellite imagery. Remote Sens (Basel) 2021;13:1868. https://doi.org/10.3390/rs13101868

[30] Du B, Mao D, Wang Z, Qiu Z, Yan H, Feng K, et al. Mapping wetland plant communities using unmanned aerial vehicle hyperspectral imagery by comparing object/pixel-based classifications combining multiple machine-learning algorithms. IEEE J Sel Top Appl Earth Obs Remote Sens 2021;14:8249–58. 10.1109/JSTARS.2021.3100923

[31] Chen J, Chen Z, Huang R, You H, Han X, Yue T, et al. The Effects of Spatial Resolution and Resampling on the Classification Accuracy of Wetland Vegetation Species and Ground Objects: A Study Based on High Spatial Resolution UAV Images. Drones 2023;7:61. https://doi.org/10.3390/drones7010061

[32] Zhou R, Yang C, Li E, Cai X, Yang J, Xia Y. Object-based wetland vegetation classification using multi-feature selection of unoccupied aerial vehicle RGB imagery. Remote Sens (Basel) 2021;13:4910. https://doi.org/10.3390/rs13234910

[33] Iyoob AL, Norbert SA, Ameer MLF, Nasar-u-Minallah M, Zahir ILM, Nuskiya MHF. Using UAV RGB Image for Object-based Feature Detection. Procedia Comput Sci 2025;260:1052–9. https://doi.org/10.1016/j.procs.2025.03.290

[34] Yang D, Zhou N, Zhu Z, Ge H, Wang W, Xu C, et al. Coastal wetland classification method based on UAV imagery: integrating hierarchical sample enhancement and multiscale sample selection techniques. Geomatics, Natural Hazards and Risk 2025;16:2585167. https://doi.org/10.1080/19475705.2025.2585167

[35] Dietenberger S, Mueller MM, Stöcker B, Dubois C, Arlaud H, Adam M, et al. Accurate Mapping of Downed Deadwood in a Dense Deciduous Forest Using UAV-SfM Data and Deep Learning. Remote Sens (Basel) 2025;17:1610. https://doi.org/10.3390/rs17091610

[36] Ameslek O, Zahir H, Latifi H, Bachaoui EM. Combining OBIA, CNN, and UAV imagery for automated detection and mapping of individual olive trees. Smart Agricultural Technology 2024;9:100546. https://doi.org/10.1016/j.atech.2024.100546

[37] Kelly M, Feirer S, Hogan S, Lyons A, Lin F, Jacygrad E. Mapping orchard trees from UAV imagery through one growing season: A comparison between OBIA-based and three CNN-based object detection methods. Drones 2025;9:593. https://doi.org/10.3390/drones9090593

[38] Iriansa, Mutmainnah. Morphological, Morphometric, and Distribution Pattern Characteristics of Optimal Harvest Phase Sago in Forest Area Based on Drone Imagery. Indonesian Journal of Social and Environmental Issues (IJSEI) 2024;5:318–34. https://doi.org/10.47540/ijsei.v5i3.1720

[39] Osozawa K. Sago palm and sago production in South Sulawesi: Essay on tropical low land development 1990. https://cir.nii.ac.jp/crid/1573387449830932736

[40] Sari DR. Agronomic Prospects for New Sago Palm Cultivation by farmers: Time to Harvest and Associated Cultivation Management. The 14th International Sago Symposium SAGO 2023 TOKYO 2023;85. https://www.sagopalmsociety.com/_files/ugd/3f58e5_398fcb790b40418ab832df78c76a3039.pdf#page=90

[41] Geng R, Jin S, Fu B, Wang B. Object-based wetland classification using multi-feature combination of ultra-high spatial resolution multispectral images. Canadian Journal of Remote Sensing 2020;46:784–802. https://doi.org/10.1080/07038992.2021.1872374

[42] Lastilla L, Belloni V, Ravanelli R, Crespi M. DSM generation from single and cross-sensor multi-view satellite images using the new agisoft metashape: The case studies of Trento and Matera (Italy). Remote Sens (Basel) 2021;13:593. https://doi.org/10.3390/rs13040593

[43] Guerra-Hernández J, Díaz-Varela RA, Ávarez-González JG, Rodríguez-González PM. Assessing a novel modelling approach with high resolution UAV imagery for monitoring health status in priority riparian forests. For Ecosyst 2021;8:61. https://doi.org/10.1186/s40663-021-00342-8

[44] Hossain MD, Chen D. Segmentation for Object-Based Image Analysis (OBIA): A review of algorithms and challenges from remote sensing perspective. ISPRS Journal of Photogrammetry and Remote Sensing 2019;150:115–34. https://doi.org/10.1016/j.isprsjprs.2019.02.009

[45] Difar HF, Abed FM. Automatic Extraction of Unmanned Aerial Vehicles (UAV)-based Cadastral Map: Case Study in AL-Shatrah District-Iraq. Iraqi Journal of Science 2022:877–96. https://doi.org/10.24996/ijs.2022.63.2.40

[46] Wenjie LIN, Yu LI, Quanhua Z. High-resolution remote sensing image segmentation using minimum spanning tree tessellation and RHMRF-FCM algorithm. 测绘学报 (英文版) 2020;3:52–63. https://doi.org/10.11947/j.JGGS.2020.0106

[47] Geng R, Jin S, Fu B, Wang B. Object-based wetland classification using multi-feature combination of ultra-high spatial resolution multispectral images. Canadian Journal of Remote Sensing 2020;46:784–802. https://doi.org/10.1080/07038992.2021.1872374

[48] Ez-zahouani B, Kharki OE, Idé SK, Zouiten M. Determination of Segmentation Parameters for Object-Based Remote Sensing Image Analysis from Conventional to Recent Approaches: A Review. International Journal of Geoinformatics 2023;19. https://doi.org/10.52939/ijg.v19i1.2497

[49] Norman M, Shahar HM, Mohamad Z, Rahim A, Mohd FA, Shafri HZM. Urban building detection using object-based image analysis (OBIA) and machine learning (ML) algorithms. IOP Conf Ser Earth Environ Sci 2021;620:012010. https://iopscience.iop.org/article/10.1088/1755-1315/620/1/012010/pdf

[50] Aposporis P. Object detection methods for improving UAV autonomy and remote sensing applications. 2020 IEEE/ACM International Conference on Advances in Social Networks Analysis and Mining (ASONAM), IEEE 2020;845–53. 10.1109/ASONAM49781.2020.9381377

[51] Demarchi L, Kania A, Ciężkowski W, Piórkowski H, Oświecimska-Piasko Z, Chormański J. Recursive Feature Elimination and Random Forest Classification of Meadows and Dry Grasslands in Lowland River Valleys of Poland Based on Airborne Hyperspectral and LiDAR Data Fusion 2020;12:1842. https://doi.org/10.3390/rs12111842

[52] Guo Q, Zhang J, Guo S, Ye Z, Deng H, Hou X, et al. Urban tree classification based on object-oriented approach and random forest algorithm using unmanned aerial vehicle (UAV) multispectral imagery. Remote Sens (Basel) 2022;14:3885. https://doi.org/10.3390/rs14163885

[53] Liu Y, Hatou K, Aihara T, Kurose S, Akiyama T, Kohno Y, et al. A robust vegetation index based on different UAV RGB images to estimate SPAD values of naked barley leaves. Remote Sens (Basel) 2021;13:686. https://doi.org/10.3390/rs13040686

[54] Neupane B, Horanont T, Hung ND. Deep learning based banana plant detection and counting using high-resolution red-green-blue (RGB) images collected from unmanned aerial vehicle (UAV). PLoS One 2019;14:e0223906. https://doi.org/10.1371/JOURNAL.PONE.0223906

[55] Xiaoqin W, Miaomiao W, Shaoqiang W, Yundong W. Extraction of vegetation information from visible unmanned aerial vehicle images. Transactions of the Chinese Society of Agricultural Engineering 2015;31:152-159. http://www.tcsae.org/en/article/doi/10.3969/j.issn.1002-6819.2015.05.022

[56] Zhang T, Su J, Xu Z, Luo Y, Li J. Sentinel-2 satellite imagery for urban land cover classification by optimized random forest classifier. Applied Sciences 2021;11:543. https://doi.org/10.3390/app11020543

[57] Ahmadi K, Kalantar B, Saeidi V, Harandi EKG, Janizadeh S, Ueda N. Comparison of machine learning methods for mapping the stand characteristics of temperate forests using multi-spectral sentinel-2 data. Remote Sens (Basel) 2020;12:3019. https://doi.org/10.3390/rs12183019

[58] Wu N, Crusiol LGT, Liu G, Wuyun D, Han G. Comparing machine learning algorithms for pixel/object-based classifications of semi-arid grassland in northern China using multisource medium resolution imageries. Remote Sens (Basel) 2023;15:750. https://doi.org/10.3390/rs15030750

[59] Erdanaev E, Kappas M, Wyss D. The Identification of Irrigated Crop Types Using Support Vector Machine, Random Forest and Maximum Likelihood Classification Methods with Sentinel-2 Data in 2018: Tashkent Province, Uzbekistan. International Journal of Geoinformatics 2022;18. https://doi.org/10.52939/ijg.v18i2.2151

[60] Hao S, Cui Y, Wang J. Segmentation scale effect analysis in the object-oriented method of high-spatial-resolution image classification. Sensors 2021;21:7935. https://doi.org/10.3390/s21237935

[61] Akcay O, Avsar EO, Inalpulat M, Genc L, Cam A. Assessment of segmentation parameters for object-based land cover classification using color-infrared imagery. ISPRS Int J Geoinf 2018;7:424. https://doi.org/10.3390/ijgi7110424

[62] Ez-zahouani B, Teodoro A, Kharki OE, Jianhua L, Kotaridis I, Yuan X, et al. Remote sensing imagery segmentation in object-based analysis: A review of methods, optimization, and quality evaluation over the past 20 years. Remote Sens Appl 2023;32:101031. https://doi.org/https://doi.org/10.1016/j.rsase.2023.101031.

[63] Sexton T, Sankaran S, Cousins AB. Predicting photosynthetic capacity in tobacco using shortwave infrared spectral reflectance. J Exp Bot 2021;72:4373–83. https://doi.org/10.1093/jxb/erab118

[64] Wang Z, Nie C, Wang H, Ao Y, Jin X, Yu X, et al. Detection and analysis of degree of maize lodging using UAV-RGB image multi-feature factors and various classification methods. ISPRS Int J Geoinf 2021;10:309. https://doi.org/10.3390/ijgi7110424

[65] Dong J, Zhang J, Zhang S, Yu Z, Song Z, Meng T. Vegetation extraction through UAV RGB imagery and efficient feature selection. PLoS One 2025;20:e0322180-. https://doi.org/https://doi.org/10.1371/journal.pone.0322180.

[66] Lai S, Li Z, Ming D, Long J, Wei Y, Zhang J. A Multi-Level Segmentation Method for Mountainous Camellia oleifera Plantation with High Canopy Closure Using UAV Imagery. Agronomy 2025;15:2522. https://doi.org/10.3390/agronomy15112522.

[67] Pranga J, Borra-Serrano I, Quataert P, Swaef TD, Nest TV, Willekens K, et al. Quantification of species composition in grass-clover swards using RGB and multispectral UAV imagery and machine learning. Front Plant Sci 2024;15:1414181. https://www.frontiersin.org/journals/plant-science/articles/10.3389/fpls.2024.1414181/full

[68] Jiménez-Lao R, Aguilar MA, Ladisa C, Aguilar FJ, Nemmaoui A. Multiresolution Segmentation For Extracting Plastic Greenhouses From Deimos-2 Imagery. Isprs Ann Photogramm Remote Sens Spatial Inf Sci 2022;2:251–8. https://doi.org/10.5194/isprs-annals-V-2-2022-251-2022.

[69] Reinprecht V, Kieffer DS. Application of UAV Photogrammetry and Multispectral Image Analysis for Identifying Land Use and Vegetation Cover Succession in Former Mining Areas. Remote Sensing 2025;17:405. https://doi.org/10.3390/RS17030405.
[70] Kior A, Yudina L, Zolin Y, Sukhov V, Sukhova E. RGB Imaging as a Tool for Remote Sensing of Characteristics of Terrestrial Plants: A Review. Plants 2024;13. https://doi.org/10.3390/plants13091262.
[71] Deng H, Zhang W, Zheng X, Zhang H. Crop Classification Combining Object-Oriented Method and Random Forest Model Using Unmanned Aerial Vehicle (UAV) Multispectral Image. Agriculture 2024;14:548. https://doi.org/10.3390/AGRICULTURE14040548.
[72] Chang B, Li F, Hu Y, Yin H, Feng Z, Zhao L. Application of UAV remote sensing for vegetation identification: a review and meta-analysis. Front Plant Sci 2025;16:1452053. https://doi.org/10.3389/FPLS.2025.1452053.
[73] Letsoin SMA, Purwestri RC, Rahmawan F, Herak D. Recognition of Sago Palm Trees Based on Transfer Learning Remote Sensing 2022;14:4932. https://doi.org/10.3390/RS14194932.
[74] Hidayat S, Matsuoka M, Baja S, Rampisela DA. Object-Based Image Analysis for Sago Palm Classification: The Most Important Features from High-Resolution Satellite Imagery. Remote Sensing 2018;10:1319. https://doi.org/10.3390/RS10081319.
[75] Sun Z, Wang Y, Pan L, Xie Y, Zhang B, Liang R, et al. Pine wilt disease detection in high-resolution UAV images using object-oriented classification. Journal of Forestry Research 2021;33:1377–89. https://doi.org/10.1007/S11676-021-01420-X.
[76] Aldaeri ASTM, Kit CY, Ting LS, Rahman MRBA. Deep Learning for Tree Crown Detection and Delineation Using UAV and High-Resolution Imagery for Biometric Parameter Extraction: A Systematic Review Forests 2026;17:179. https://doi.org/10.3390/f17020179 https://www.mdpi.com/1999-4907/17/2/179
[77] Eskandari R, Mahdianpari M, Mohammadimanesh F, Salehi B, Brisco B, Homayouni S. Meta-analysis of Unmanned Aerial Vehicle (UAV) Imagery for Agro-environmental Monitoring Using Machine Learning and Statistical Models. Remote Sensing 2020;12:3511. https://doi.org/10.3390/RS12213511.
[78] Feng C, Zhang W, Deng H, Dong L, Zhang H, Tang L, et al. A combination of OBIA and random forest based on visible UAV remote sensing for accurately extracted information about weeds in areas with different weed densities in farmland. Remote Sens (Basel) 2023;15:4696. https://doi.org/10.3390/rs15194696
[79] Räsänen A, Virtanen T. Data and resolution requirements in mapping vegetation in spatially heterogeneous landscapes. Remote Sens Environ 2019;230:111207. https://doi.org/10.1016/J.RSE.2019.05.026.
[80] Dimara PA, Auri A. Effect of Landform on the Distribution of Metroxylon sagu Habitat in Yapen Islands, Papua Province, Indonesia. Jurnal Sylva Lestari 2023;11:79–97. https://doi.org/10.23960/JSL.V11I1.633.